JOURNAL OF COMPUTATIONAL PHYSICS 109, 67–75 (1993)

High Strain Lagrangian Hydrodynamics

A Three-Dimensional SPH Code for Dynamic Material Response

LARRY D. LIBERSKY

Center for Explosives Technology Research (CETR), New Mexico Institute of Mining and Technology, Socorro, New Mexico 87801 and Space Kinetic Impacts and Debris Branch, Phillips Laboratory, Kirtland, New Mexico 87117

ALBERT G. PETSCHEK

Department of Physics, New Mexico Institute of Mining and Technology, Socorro, New Mexico 87801

THEODORE C. CARNEY AND JIM R. HIPP

Advanced Sciences Incorporated (ASI), 6739 Academy Road NE, Albuquerque, New Mexico 87109

AND

FIROOZ A. ALLAHDADI

Space Kinetic Impacts and Debris Branch (PL/WSSD), Phillips Laboratory, Kirtland, New Mexico 87117

Received December 11, 1991; revised March 11, 1993

MAGI, a three-dimensional shock and material response code which is based on smoothed particle hydrodynamics (SPH) is described. Calculations are presented and compared with experimental results. The SPH method is unique in that it employs no spatial mesh. The absence of a grid leads to some nice features such as the ability to handle large distortions in a pure Lagrangian frame and a natural treatment of voids. Both of these features are important in the tracking of debris clouds produced by hypervelocity impact—a difficult problem for which SPH seems ideally suited. We believe this is the first application of SPH to the dynamics of elastic-plastic solids.

INTRODUCTION

Traditionally, Lagrangian codes have been used to simulate material response when the amount of deformation is small. When the deformation is large, Eulerian calculations have been employed. The Lagrangian calculation is more accurate—the Eulerian calculation has greater applicability. These strengths and weaknesses are due to the convective derivative which is absent in the equations written in the moving Lagrangian frame. Numerical treatment of this advection term is difficult and introduces inaccuracies into the calculation. However, if the errors can be made small, the Eulerian calculation can be used to treat a variety of high strain phenomena.

Various methods have been devised in order to achieve the best features of both approaches. Such "hybrid" techniques normally use two grids, one Lagrangian—the other Eulerian, with information exchanged between them. These mappings add a good deal of complexity to the calculation and can also introduce inaccuracies. Nevertheless, many hybrid techniques have been successful and are widely used today.

Unique in computational fluid dynamics is smoothed particle hydrodynamics (SPH). The SPH technique uses no underlying grid—it is a pure Lagrangian particle method developed by Lucy [1], Gingold [2, 3], Monaghan [4–6], and Benz [7]. The absence of a mesh and the calculation of interactions among particles based on their separation alone means that large deformations can be computed without difficulty. It is for this reason that SPH has the potential to be a valuable computational tool. Although SPH has been proven excellent for astrophysical applications, it has not been applied to problems requiring the entire stress tensor. This paper addresses the extension of SPH to such problems.

0021-9991/93 $5.00

THE METHOD

The foundation of SPH is interpolation theory. The conservation laws of continuum fluid dynamics, in the form of partial differential equations, are transformed into integral equations through the use of an interpolation function that gives the "kernel estimate" of the field variables at a point. Computationally, information is known only at discrete points, so that the integrals are evaluated as sums over neighboring points. The reason that an underlying grid is not needed is that functions are evaluated using their values at the discrete points (particles) and an interpolation kernel. An integration by parts then moves spatial derivatives from operating on the physical quantities to operating on the interpolation kernel which is analytic. These concepts will now be described more fully. Consider a function f, a kernel W which has a width measured by the parameter h, and the following equation:

$$\langle f(\mathbf{x})\rangle = \int W(\mathbf{x}-\mathbf{x}', h)\, f(\mathbf{x}')\, d\mathbf{x}'. \tag{1}$$

We find it useful to employ both tensor (superscripted) and vector (bold) notation. For non-negative W with integral normalized to unity, it follows that

$$\langle f(\mathbf{x})\rangle \xrightarrow[h\to 0]{} f(\mathbf{x}). \tag{2}$$

Relation (1) therefore may be considered to define the kernel estimate $\langle f\rangle$ of f. It is accurate to order $h^2\nabla^2 f$ [7]. If W is the Dirac delta function then we have the equality $\langle f\rangle = f$. Now suppose that f is known only at N discrete points that are spatially distributed according to the number density distribution

$$n(\mathbf{x}) = \sum_{j=1}^{N} \delta(\mathbf{x}-\mathbf{x}_j). \tag{3}$$

If we associate with particle j a volume

$$d\mathbf{x}' = \frac{m_j}{\rho(\mathbf{x}_j)}, \tag{4}$$

thus introducing the concept of particle mass (m), then an approximation to (1) is

$$\langle f(\mathbf{x})\rangle \cong \sum_{j=1}^{N} f_j W(\mathbf{x}-\mathbf{x}_j, h)\frac{m_j}{\rho_j}. \tag{5}$$

This approximation to functions will allow us to estimate accelerations, strain rates, etc. in Euler's equations (or the Navier–Stokes equations) and forms the basis of SPH. For a detailed discussion see Benz [7].

DERIVATION OF THE SPH EQUATIONS

The conservation equations of continuum mechanics are:

$$\frac{d\rho}{dt} = -\rho\frac{\partial U^\beta}{\partial x^\beta} \tag{6}$$

$$\frac{dU^\alpha}{dt} = -\frac{1}{\rho}\frac{\partial \sigma^{\alpha\beta}}{\partial x^\beta} \tag{7}$$

$$\frac{dE}{dt} = -\frac{\sigma^{\alpha\beta}}{\rho}\frac{\partial U^\alpha}{\partial x^\beta} \tag{8}$$

$$\frac{dx^\alpha}{dt} = U^\alpha. \tag{9}$$

Dependent variables are the scalar density (ρ) and specific internal energy (E), the velocity components U^α, and the stress tensor $\sigma^{\alpha\beta}$. The independent variables are the spatial coordinates x^β and the time t. The total time derivative (d/dt) is taken in the moving Lagrangian frame. Summation over repeated Greek indices is implied. Let us now cast Eqs. (6)–(8) into the SPH framework by applying the procedure outlined above. Following Monaghan [8] we rewrite the momentum and energy equations; then we find the kernel estimate. The result is

$$\int W\frac{d\rho}{dt}\,d\mathbf{x}' = -\int W\rho\frac{\partial U^\beta}{\partial x'^\beta}\,d\mathbf{x}' \tag{10}$$

$$\int W\frac{dU^\alpha}{dt}\,d\mathbf{x}' = -\int W\frac{\partial}{\partial x'^\beta}\left(\frac{\sigma^{\alpha\beta}}{\rho}\right)d\mathbf{x}' - \int W\frac{\sigma^{\alpha\beta}}{\rho^2}\frac{\partial\rho}{\partial x'^\beta}\,d\mathbf{x}' \tag{11}$$

$$\int W\frac{dE}{dt}\,d\mathbf{x}' = -\int W\frac{\sigma^{\alpha\beta}}{\rho^2}\frac{\partial\rho U^\alpha}{\partial x'^\beta}\,d\mathbf{x}' + \int W\frac{\sigma^{\alpha\beta}U^\alpha}{\rho^2}\frac{\partial\rho}{\partial x'^\beta}\,d\mathbf{x}'. \tag{12}$$

We now linearize these equations by taking integrals of products equal to products of integrals (an approximation accurate to order h^2 times the product of the gradients of the functions [7]) and drop the kernel estimates for quantities that do not involve spatial derivatives to obtain

$$\int W\frac{d\rho}{dt}\,d\mathbf{x}' \approx -\rho(\mathbf{x})\int W\frac{\partial U^\beta}{\partial x'^\beta}\,d\mathbf{x}' \tag{13}$$

$$\int W\frac{dU^\alpha}{dt}\,d\mathbf{x}' \approx -\int W\frac{\partial}{\partial x'^\beta}\left(\frac{\sigma^{\alpha\beta}}{\rho}\right)d\mathbf{x}' - \frac{\sigma^{\alpha\beta}(\mathbf{x})}{\rho^2(\mathbf{x})}\int W\frac{\partial\rho}{\partial x'^\beta}\,d\mathbf{x}' \tag{14}$$

$$\int W\frac{dE}{dt}\,d\mathbf{x}' \approx -\frac{\sigma^{\alpha\beta}(\mathbf{x})}{\rho^2(\mathbf{x})}\int W\frac{\partial \rho U^\alpha}{\partial x'^\beta}\,d\mathbf{x}' + \frac{\sigma^{\alpha\beta}(\mathbf{x})\,U^\alpha(\mathbf{x})}{\rho^2(\mathbf{x})}\int W\frac{\partial \rho}{\partial x'^\beta}\,d\mathbf{x}'. \quad (15)$$

The remaining kernel estimates are now integrated by parts, assuming W approaches zero fast enough that the surface terms vanish:

$$\int W\frac{d\rho}{dt}\,d\mathbf{x}' \approx \rho(\mathbf{x})\int U^\beta\frac{\partial W}{\partial x'^\beta}\,d\mathbf{x}' \quad (16)$$

$$\int W\frac{dU^\alpha}{dt}\,d\mathbf{x}' \approx \int\frac{\sigma^{\alpha\beta}}{\rho}\frac{\partial W}{\partial x'^\beta}\,d\mathbf{x}' + \frac{\sigma^{\alpha\beta}(\mathbf{x})}{\rho^2(\mathbf{x})}\int \rho(\mathbf{x}')\frac{\partial W}{\partial x'^\beta}\,d\mathbf{x}' \quad (17)$$

$$\int W\frac{dE}{dt}\,d\mathbf{x}' \approx \frac{\sigma^{\alpha\beta}(\mathbf{x})}{\rho^2(\mathbf{x})}\int \rho(\mathbf{x}')\,U^\alpha(\mathbf{x}')\frac{\partial W}{\partial x'^\beta}\,d\mathbf{x}' - \frac{\sigma^{\alpha\beta}(\mathbf{x})\,U^\alpha(\mathbf{x})}{\rho^2(\mathbf{x})}\int \rho(\mathbf{x}')\frac{\partial W}{\partial x'^\beta}\,d\mathbf{x}'. \quad (18)$$

Finally, the integrals are evaluated by the particle method, Eq. (5), to give

$$\frac{d\rho_i}{dt} = \rho_i\sum_j\frac{m_j}{\rho_j}(U_i^\beta - U_j^\beta)\,W_{ij,\beta} \quad (19)$$

$$\frac{dU_i^\alpha}{dt} = -\sum_j m_j\left(\frac{\sigma_i^{\alpha\beta}}{\rho_i^2}+\frac{\sigma_j^{\alpha\beta}}{\rho_j^2}\right)W_{ij,\beta} \quad (20)$$

$$\frac{dE_i}{dt} = \frac{\sigma_i^{\alpha\beta}}{\rho_i^2}\sum_j m_j(U_i^\alpha - U_j^\alpha)\,W_{ij,\beta}. \quad (21)$$

We have introduced the notation $W_{ij} = W(\mathbf{x}_i - \mathbf{x}_j, h)$ and $\partial W_{ij}/\partial x_i^\beta = W_{ij,\beta}$. In obtaining (19) we subtracted from (13) the term

$$\rho_i U_i^\beta\int\frac{\partial W}{\partial x_i^\beta}\,d^3\mathbf{x}' \cong \rho_i U_i^\beta\sum_j\frac{m_j}{\rho_j}W_{ij,\beta}, \quad (22)$$

which is zero because the kernel vanishes at infinity. In this way we introduce velocity differences into the density calculation, which is desirable to maintain Galilean invariance and to be consistent with the energy calculation in (21). Velocity differences entered the energy equation through the rewriting in (12). The rewriting in (11) produced the symmetry between i and j in (20) which ensures the satisfaction of Newton's third law. Equations (19)–(21) are the conservation laws of continuum dynamics written in the SPH framework. A given particle i has a density determined by (19), an acceleration obtained from (20), and an internal energy change given by (21). The summations are over neighboring j particles. These equations are not unique. Several other forms of particle equations can be derived using various mathematical manipulations. Some of these are discussed by Monaghan [9].

THE DENSITY CALCULATION

It is important to recognize that (19) is not the density calculation that normally appears in the SPH literature. It is more in the spirit of SPH to compute the density using the equation obtained by substituting ρ for f in (5), namely,

$$\rho_i = \sum_j m_j W_{ij}. \quad (23)$$

With this equation only particle coordinates and masses are required to compute the density, and the continuity equation (6) is automatically satisfied. The disadvantage of using (23) is edge effects—particles near a free surface appear underdense and therefore in tension, causing motion. Benz [7] discusses several possible solutions to this problem including spacing modification, ghost particles, initial relaxation, and the use of (19). Note that using the chain rule on (23) and subtracting (22) leads to

$$\frac{d\rho_i}{dt} = \rho_i\sum_j\frac{m_j}{\rho_i}(U_i^\beta - U_j^\beta)\,W_{ij,\beta} \quad (24)$$

which differs from (19) only in that ρ_i appears in the denominator rather than ρ_j. We have not yet explored the consequences of using (24) in place of (19). The difference is of the same order as the difference between the product of the expected values and the expected value of the product.

ARTIFICIAL VISCOSITY AND WALL HEATING

As they stand, Eqs. (19)–(21) yield large unphysical oscillations near shocks. In fact, many numerical solutions of the continuum equations will exhibit this behavior because the dissipative terms have been omitted. Variations of physical quantities across shocks in nature are far too sharp to be captured by numerical techniques. Von Neumann and Richtmyer [10] invented "artificial viscosity" which acts to smooth shocks over a few resolution lengths and to stabilize numerical solutions. The additional term is introduced into the equations as an artificial viscous pressure Π. We follow Monaghan and Gingold [4] who derived the artificial viscous pressure for SPH,

$$\Pi_{ij} = \begin{cases}\dfrac{-\alpha\bar{c}_{ij}\mu_{ij}+\beta\mu_{ij}^2}{\bar{\rho}_{ij}} & \text{if } (\mathbf{U}_i-\mathbf{U}_j)\cdot(\mathbf{x}_i-\mathbf{x}_j)<0\\ 0 & \text{otherwise,}\end{cases} \quad (25)$$

where

$$\mu_{ij}=\frac{h(\mathbf{U}_i-\mathbf{U}_j)\cdot(\mathbf{x}_i-\mathbf{x}_j)}{(\mathbf{x}_i-\mathbf{x}_j)^2+\varepsilon h^2} \tag{26}$$

and

$$\bar{c}_{ij}=(c_i+c_j)/2, \qquad \bar{\rho}_{ij}=(\rho_i+\rho_j)/2. \tag{27}$$

The parameters α and β appearing in (25) are of order unity [11, 12] and ε in (26) is usually taken as 0.1 [11]. The linear term in (25) uses the sound speed c. This artificial viscosity gives satisfactory results in most cases, but under some severe conditions it fails to remove spurious heating. An example of this is when a stream of gas is brought to rest against a rigid wall. Noh [13] was able to improve numerical solutions in such cases dramatically by adding an artificial heat conduction term to the energy equation. Monaghan [14] derived the SPH analog of Noh's "wall heating" term in which the net artificial heat flux at particle i is given by

$$H_i=2\sum_j \frac{\bar{\zeta}_{ij}}{\bar{\rho}_{ij}}\frac{E_i-E_j}{x_{ij}^2}\mathbf{x}_{ij}\cdot\nabla_i W_{ij}, \tag{28}$$

where

$$\bar{\zeta}_{ij}=(\zeta_i+\zeta_j)/2, \qquad \mathbf{x}_{ij}=\mathbf{x}_i-\mathbf{x}_j, \tag{29}$$

and

$$\zeta=g_1 hc+g_2 h^2(|\nabla\cdot\mathbf{U}|-\nabla\cdot\mathbf{U}). \tag{30}$$

The two parameters appearing in (30) are of order unity [14]. The particle equations with the artificial viscosity and artificial heat conduction terms included are

$$\frac{d\rho_i}{dt}=\rho_i\sum_j\frac{m_j}{\rho_j}(U_i^\beta-U_j^\beta)W_{ij,\beta} \tag{31}$$

$$\frac{dU_i^\alpha}{dt}=-\sum_j m_j\left(\frac{\sigma_i^{\alpha\beta}}{\rho_i^2}+\frac{\sigma_j^{\alpha\beta}}{\rho_j^2}+\Pi_{ij}\right)W_{ij,\beta} \tag{32}$$

$$\frac{dE_i}{dt}=\sum_j m_j(U_i^\alpha-U_j^\alpha)\left(\frac{\sigma_i^{\alpha\beta}}{\rho_i^2}+\frac{1}{2}\Pi_{ij}\right)W_{ij,\beta}+H_i. \tag{33}$$

CONSTITUTIVE RELATIONS

The stress tensor appearing in Eqs. (32) and (33) is defined in terms of an isotropic part which is the pressure (P) and the traceless symmetric deviatoric stress (S):

$$\sigma^{\alpha\beta}=P\,\delta^{\alpha\beta}-S^{\alpha\beta}. \tag{34}$$

The pressure is normally computed using an equation of state having functional form $P=P(\rho, E)$, such as the Mie–Gruneisen equation for solids or gamma-law for gases:

Mie–Gruneisen, $$P(\rho, E)=(1-\tfrac{1}{2}\Gamma\eta)\,P_H(\rho)+\Gamma\rho E \tag{35}$$

$$P_H=\begin{cases}a_0\eta+b_0\eta^2+c_0\eta^3, & \eta>0,\\ a_0\eta, & \eta<0;\end{cases} \tag{36}$$

Ideal Gas, $$P=(\gamma-1)\,\rho E. \tag{37}$$

The subscript "H" refers to the Hugoniot curve, while $\eta=\rho/\rho_0-1$ is used to represent the compression and Γ is the Gruneisen parameter. The constants a_0, b_0, and c_0 in (36) can be related to the parameters C and S in the linear shock velocity—particle velocity relation $U_S=C+SU_p$ through a Taylor's expansion of the Hugoniot curve $P_H=C^2\eta(1+\eta)/[1-\eta(S-1)]^2$:

$$a_0=\rho_0 C^2 \tag{38}$$

$$b_0=a_0[1+2(S-1)] \tag{39}$$

$$c_0=a_0[2(S-1)+3(S-1)^2]. \tag{40}$$

For the anisotropic part of (34) we write a prognostic equation for the deviatoric stress, assuming small displacements

$$\dot{S}^{\alpha\beta}=\mu\bar{\dot{\varepsilon}}^{\alpha\beta}=\mu(\dot{\varepsilon}^{\alpha\beta}-\tfrac{1}{3}\delta^{\alpha\beta}\dot{\varepsilon}^{\gamma\gamma}), \tag{41}$$

where μ is the shear modulus and $\bar{\dot{\varepsilon}}$ is the traceless rate of strain. However, for finite displacements this equation is not material frame indifferent [15]; that is, the material response will depend in an unphysical way on rotations (and possibly translations) of the material and of the observer describing it. A variety of frame-indifferent stress rates have been formulated. Herrmann [16] examines the relative merits of several of these. The Jaumann rate is the most widely used in codes and we adopt it also. With the Jaumann rate, our constitutive equation is

$$\dot{S}^{\alpha\beta}-S^{\alpha\gamma}\dot{R}^{\beta\gamma}-\dot{S}^{\gamma\beta}\dot{R}^{\alpha\gamma}=\mu\bar{\dot{\varepsilon}}^{\alpha\beta}. \tag{42}$$

The strain rate and rotation rate tensors that have been used are defined as

$$\dot{\varepsilon}^{\alpha\beta}=\frac{1}{2}\left(\frac{\partial U^\alpha}{\partial x^\beta}+\frac{\partial U^\beta}{\partial x^\alpha}\right),$$
$$\dot{R}^{\alpha\beta}=\frac{1}{2}\left(\frac{\partial U^\alpha}{\partial x^\beta}-\frac{\partial U^\beta}{\partial x^\alpha}\right). \tag{43}$$

Particle equations for (43) are obtained by Libersky and Petschek [17] in a manner similar to that of (19, 20, 21)

$$\frac{dS^{\alpha\beta}}{dt} - S_i^{\alpha\gamma}\dot{R}_i^{\beta\gamma} - \dot{S}_i^{\gamma\beta}\dot{R}_i^{\alpha\gamma} = \frac{\mu}{2}\sum_j \frac{m_j}{\rho_j}\Big[(U_j^\alpha - U_i^\alpha)\, W_{ij,\beta} + (U_j^\beta - U_i^\beta)\, W_{ij,\beta} - \frac{1}{3} D_i\, \delta^{\alpha\beta}\Big]. \tag{44}$$

The divergence is already determined by (19), $D_i = \dot{\rho}_i/\rho_i$, and the rotation rate is

$$\dot{R}_i^{\alpha\beta} = \sum_j \frac{m_j}{\rho_j}[(U_j^\alpha - U_i^\alpha)\, W_{ij,\beta} - (U_j^\beta - U_i^\beta)\, W_{ij,\beta}]. \tag{45}$$

The plastic flow regime is determined by the von Mieses criterion when the second stress invariant $J^2 = S^{\alpha\beta}S^{\alpha\beta}$ exceeds the known flow stress (Y_0). The individual deviators are then brought back to the flow surface,

$$S^{\alpha\beta} = S^{\alpha\beta}\sqrt{Y_0/3J^2}. \tag{46}$$

A more accurate treatment for most metals, not yet implemented in our code, is obtained by computing a history-sensitive flow stress, rather than a predetermined fixed value as described above. The Johnson–Cook model [18], for example, takes into account thermal softening, strain hardening, and strain rate effects on the equivalent flow stress. This more sophisticated model contains seven strength-related parameters. The elastic-perfectly plastic constitutive model described above contains two parameters, the shear modulus (μ) and the plastic yield stress (Y_0).

THE KERNEL

The interpolation kernel or smoothing function most widely used in three-dimensional SPH is the B-spline,

$$W_4(v, h) = \begin{cases} \frac{15}{7}(\frac{2}{3} - v^2 + \frac{1}{2}v^3) & 0 < v < 1 \\ \frac{5}{14}(2-v)^3 & 1 < v < 2 \\ 0 & \text{otherwise.} \end{cases} \tag{47}$$

In Eq. (47) $v = |\mathbf{x}_i - \mathbf{x}_j|/h$, while the fractional coefficients assure proper normalization and continuity. This kernel interpolates to second order in h and is always non-negative. The kernel also has compact support; that is, it goes to zero at a distance $2h$ from its peak. This provides a clear limit on the number of neighbor particles. Higher order interpolation kernels exist [3, 7] but are not always positive definite.

It is important to note that the smoothing length h in (47) need not be constant but can be a function of space and time. Variable smoothing length is the SPH analog to adaptive gridding in mesh-based codes allowing greater resolution in regions where it is needed. Some calculations are difficult to perform with SPH unless a variable smoothing length is used. For example, in expanding particle clouds, such as would be produced by explosions and hypervelocity impact of thin plates, h must increase in order to maintain adequate resolution. When the use of variable h is appropriate we use the method discussed by Benz [7] in which the smoothing length changes according to the rate equation $\dot{h}/h = \frac{1}{3}\nabla \cdot \mathbf{V}$. Bicknell [19] shows that $h = h(t)$ conserves the momentum but $h = h(\mathbf{x})$ does not. The error introduced by the spatial dependence does not appear to be significant.

TIME INTEGRATION

Equations (31)–(33), (44) are integrated using a standard leap-frog algorithm [11] with the time step calculated from the configuration at time t to advance the field variables to $t + \delta t$. We will switch from superscript tensor indices to subscripts here in order to accommodate the standard superscript representation of the time stepping in which n indicates the current time t and $n+1$ indicates the advanced time $t + \delta t$:

$$\rho^{n+1} = \rho^n(1 - D\,\delta t) \tag{48}$$

$$U_\alpha^{n+1/2} = U_\alpha^{n-1/2} + \tfrac{1}{2}(\delta t^n + \delta t^{n-1})\, F \tag{49}$$

$$E^{n+1} = E^n + \delta t^n G \tag{50}$$

$$S_{\alpha\beta}^{n+1} = S_{\alpha\beta}^n + \delta t^n H \tag{51}$$

$$x_\alpha^{n+1} = x_\alpha^n + U_\alpha^{n+1/2}\,\delta t^n. \tag{52}$$

In these equations D, F, G, and H represent the volumetric strain, total acceleration, work per unit mass, and stress rate on a particle as determined by the interactions with neighbor particles. The accuracy of the leap-frog scheme is second order in time and its stability is guaranteed by using the Courant–Friedrichs–Lewy condition to determine the size of the time step δt. We find the minimum over all particles of $\omega h/(c+s)$, where c is the adiabatic sound speed, s is the particle speed, h is the smoothing length, and ω is a constant factor. Choosing $\omega = 0.3$ seems adequate.

FINDING NEIGHBORS

The N^2 interactions that result from direct application of the SPH formalism without consideration of the finite range of the smoothing function can be reduced to $\sim N \log N$ through use of a "linked-list" [20]. The linked list algorithms perform three basic functions in our code: spatial

sorting, construction of particle interaction lists and ghost particle generation. Ghost particles are fictitious particles used to impose boundary conditions. All sorting activities are facilitated by means of an identifying particle number assigned when the particles are generated.

Spatial sorting is accomplished by embedding a uniform grid within the computational domain and assigning particles to the grid boxes. The sides of each box have length equal to the range of the smoothing function. Possible neighbors for a particle are those occupying the same box and the neighboring boxes. Thus, only nine boxes need be considered in 2D and 27 in 3D. Both real and ghost boxes (fictitious cells adjacent to the computational domain) are generated. Ghost boxes contain ghost particles formed by reflections at the computational boundary.

CALCULATIONS

The Noh Problem

The uniform implosion of an ideal gas was conceived by Noh [13] as a stringent test problem for shock codes. Initially, the gas is moving radially inward at unit speed, unit density, and zero internal energy. For $\gamma = \frac{5}{3}$ and spherical symmetry, Noh found the analytic solution to be a shock moving radially outward at speed $\frac{1}{3}$. The gas behind the shock has particle speed 0, specific internal energy $\frac{1}{2}$, and density 64. The value of 64 is due to a 16-fold increase from adiabatic compression and a four-fold increase across a strong shock. Our calculation used one-eighth of a sphere in three-dimensional Cartesian coordinates and three

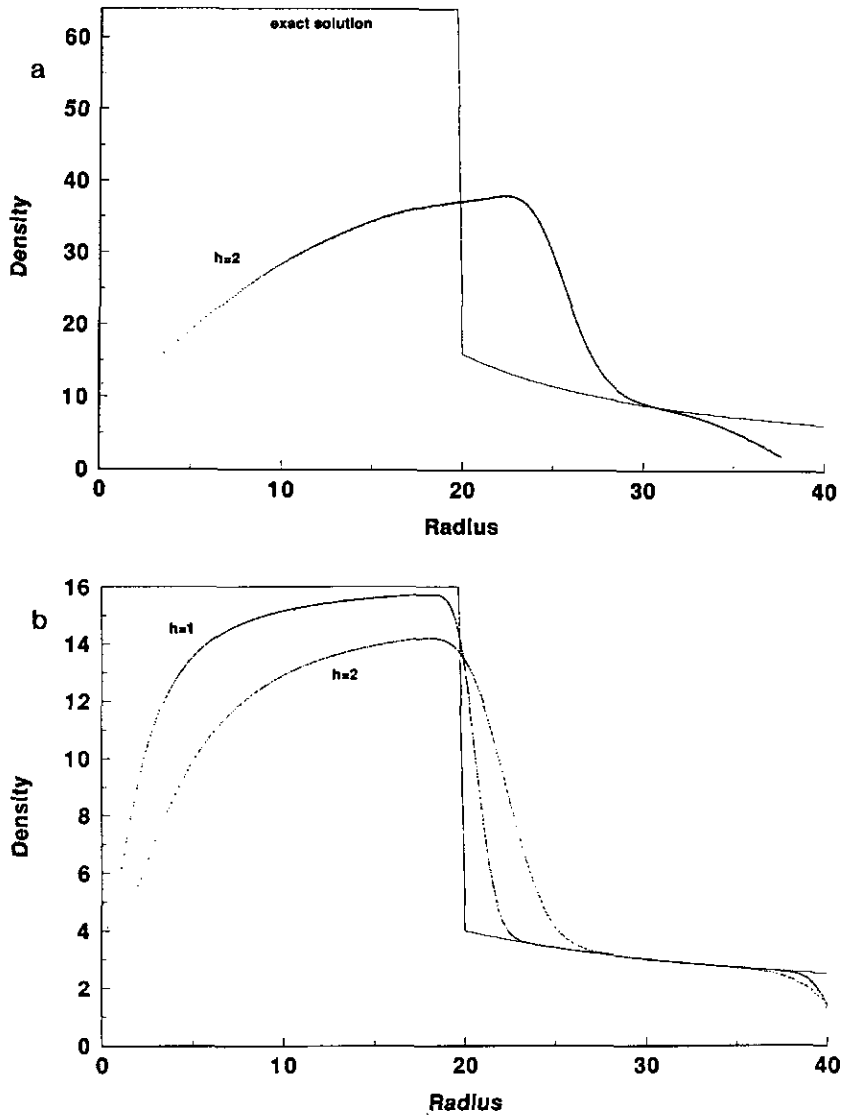

FIG. 1. (a) Density profile at $t = 60$ for the spherical Noh implosion problem as computed with 3D Cartesian SPH, using a smoothing length of two. The exact solution is also plotted. (b) Density profiles at $t = 60$ for the cylindrical Noh implosion problem as computed with 2D Cartesian SPH. Results of two calculations, corresponding to different values of the smoothing length and the exact solution are shown.

reflecting planes. Particles were placed within this domain in a regular cubic array and then randomly perturbed with maximum excursion of $h/8$. The initial radius of the particle cloud was 90. The smoothing length was set to 2 with 1.5 particles per h in each coordinate direction giving 187,688 particles, including ghost particles. Each particle was given unit density, unit speed inward, and zero internal energy. Results of the SPH calculation are shown in Fig. 1a, where the density is plotted as a function of radius for each particle at time 60. Note that all SPH particles fall on one curve, showing that symmetry is achieved in the calculation. This is the result to be expected as there is no spatial mesh which can bias the solution along gridlines. The calculation took 130 h to run on a 15 Mflop worstation. This is a relatively long time, we suspect, compared to other methods. The reason for the slowness is the implosion nature of the problem, coupled with our use of a constant smoothing length. As the gas continues to move radially inward, the calculational time increases dramatically as the number of interacting neighbors for each particle increases by a factor of 64 because the particles are piling up near the origin but the smoothing length remains fixed. An SPH calculation with a variable smoothing length would prove much more efficient for this problem. For explosions and rarefactions the variable smoothing length is often required in order to maintain resolution in an expanding particle cloud. We also present results of the "cylindrical" Noh problem in Fig. 1b. In this geometry the gas behind the shock should have particle speed 0, specific internal energy $\frac{1}{2}$, and density 16. Two runs were performed using different values (1.0, 2.0) for the smoothing length and two particles per h. One reflecting plane and a half-circle of particles were employed. The low resolution calculation used 15,482 particles and the higher resolution, 60,000. The run times were 4.7 and 23 h, respectively, on a 15 Mflop workstation. Results of all these "Noh" problems are given in Fig. 1.

TABLE I

Properties of Materials Used in the Calculations

	ρ_0 (g/cc)	C (cm/μs)	S	μ (Mb)	Y_0 (Kb)	Γ
Copper	8.93	0.39	1.50	0.46	4.50	2.00
Aluminum	2.71	0.53	1.50	0.25	5.50	1.70
Iron	7.89	0.36	1.80	0.80	5.00	1.81

Cylinder Impact Test

Numerical simulation of the deformation of a metal cylinder resulting from normal impact against a flat, rigid surface is often used to test constitutive models in codes. There is ample experimental data and the tests are simple yet stringent. We have modeled an ARMCO iron cylinder with speed 221 m/s, impacting a perfectly reflecting surface using SPH. One-quarter of the cylinder and two reflecting planes were used. A third reflecting plane represented a perfectly rigid boundary. The initial length of the iron rod was $L_0 = 2.54$ cm and the initial diameter was $D_0 = 0.76$ cm. The smoothing length was chosen to be $h = 0.038$ cm with one particle-per-h in each coordinate direction. A total of 6097

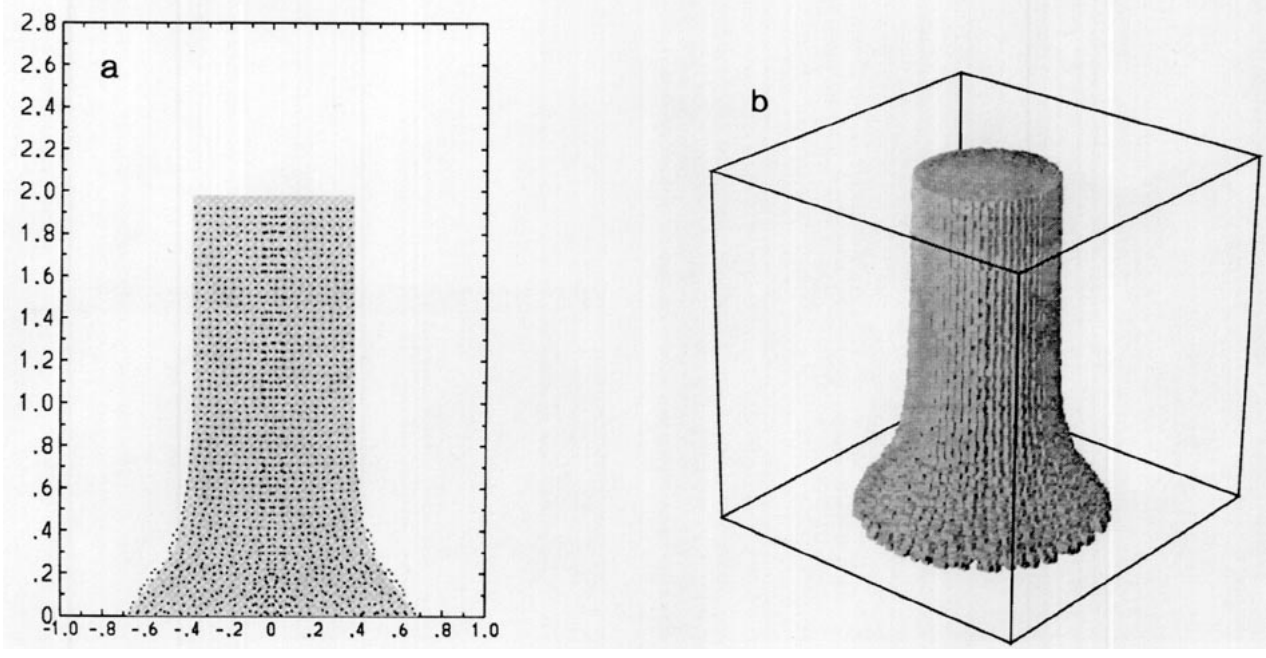

FIG. 2. Cylinder impact test with ARMCO iron at 221 m/s: (a) Calculation (dots) and experiment (shaded area). (b) 3D rendering of the SPH calculated cylinder.

particles were used in the simulation. Material properties used are given in Table I. Figure 2a shows the final shape of the computed cylinder (dots) and the actual cylinder (shaded area). The experimental data were obtained from [21]. Figure 2b is a three-dimensional rendering of the SPH computed cylinder. Reasonable agreement with experiment is observed. We have not investigated the sensitivity of the calculation to the artificial viscosity parameters ($\alpha = 2.5$, $\beta = 2.5$) or the artificial heat conduction parameters ($g_1 = 0.5$, $g_2 = 1.0$). The calculation was run to 60 μs at which time all motions were negligible. The calculation took 1980 cycles and 6 h on a 15 Mflop workstation.

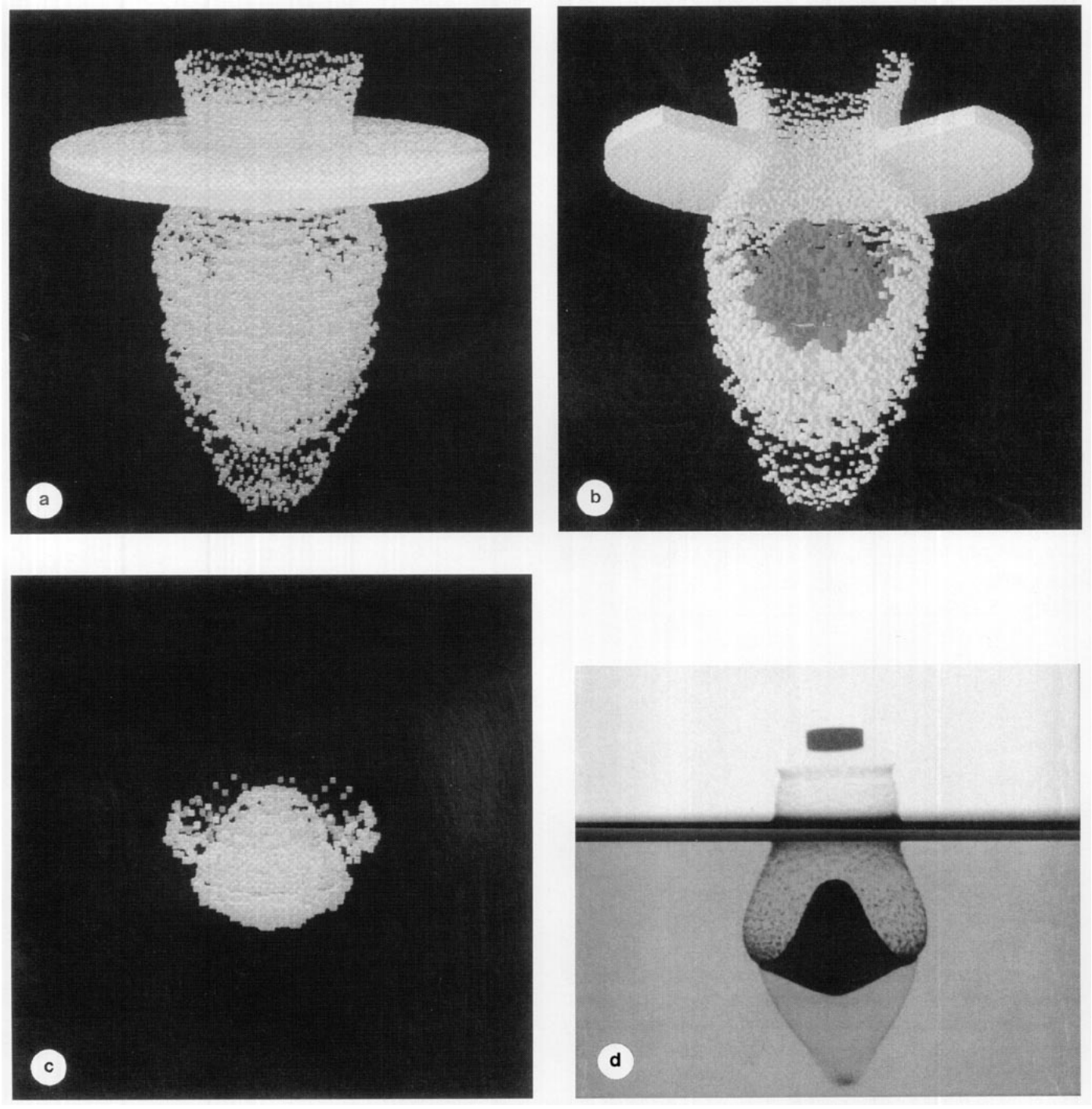

FIG. 3. Debris cloud produced by the impact of a copper pellet on an aluminum bumper plate: (a) SPH calculation viewed from above the plate. (b) SPH calculation viewed from below the plate. (c) SPH calculation. Copper projectile particles only. (d) Experimental X-ray photograph [20].

Hypervelocity Impact

Figure 3 shows the debris cloud resulting from the nearly normal impact of a 3-g copper disk (11.18-mm diameter × 3.45-mm thick) on a 2.87-mm thick aluminum bumber plate at 5.55 km/s. Figure 3d is a radiograph of the actual cloud at 6.40 μs after impact with a 5.4° yaw, courtesy of A. J. Piekutowski [22]. The SPH-computed debris clouds for normal impact are shown from views above Fig. 3a and below Fig. 3b the plate. Both aluminum plate particles and copper projectile particles are displayed in 3a but the copper particles are mostly hidden inside the cloud of aluminum. In 3b a wedge of particles has been removed from the plot so that the interior of the cloud and both materials can be seen. We have displayed only copper particles in Fig. 3c. The two materials are easily distinguished in the X-ray photograph (Fig. 3d). The SPH result compares favorably with the experiment in that the maximum width and length of the debris clouds agree. This result is to be compared with the two-dimensional axi-symmetric calculation presented in the companion paper "Cylindrical Smoothed Particle Hydrodynamics" appearing in this volume. The greater resolution permitted by the 2D calculation allowed the code to capture fine details of the experiment with remarkable sharpness. Some of these features such as the "kink" in the cloud at the aluminum–copper interface is missing in the 3D simulation. Material properties used in the calculation are given in Table I. We took $h = 0.72$ mm in the plate and $h = 0.86$ mm in the projectile with 1.5 particles per h in both, giving a total of 30,583 particles. Only one quadrant of the problem was computed as we employed two reflecting planes. The calculation took 260 cycles and 10 h on a 15 Mflop workstation.

DISCUSSION

The three-dimensional SPH code *MAGI* has been described and three calculations presented. The calculated density for the Noh problem ($\rho = 38$) falls well short of the analytic solution ($\rho = 64$) due to the coarse resolution used. However, the solution is well behaved, perfect symmetry is maintained, and we expect to see the solution improve with use of finer resolution. Results for the cylinder impact calculation agree reasonably well with experiment. The hypervelocity impact calculation is in good agreement with experiment, reproducing the distinctive shapes of the deformed projectile and plate debris cloud. This 3D result is not as good as the 2D axisymmetric calculation presented in the companion paper "Cylindrical Smoothed Particle Hydrodynamics" appearing in this volume. We are able to use a much smaller smoothing length and more particles in the 2D calculation and, therefore, capture fine details of the debris cloud remarkably well. We have no reason to doubt that the same accuracy could be achieved in the 3D calculation with equivalent resolution. Such a calculation is not practical on today's workstations.

We are encouraged by these results (and those of the companion paper as well), but recognize the need for improvement to the constitutive modeling and the viscosity. Advantages of the method are its robustness, conceptual simplicity, ease of adding new physics, a natural treatment of void, and the ability to handle high strains in a pure Lagrangian frame. Tracking of debris clouds resulting from hypervelocity impacts is a particularly important advanage of the method.

ACKNOWLEDGMENTS

Steve Andreson contributed much in the building of the code. We have benefited from discussions with Dr. Stellingwerf and Professor Benz. We thank Dr. Per-Anders Persson of New Mexico Tech for his support of this work.

REFERENCES

1. L. B. Lucy, *Astron. J.* **83**, 1013 (1977).
2. R. A. Gingold and J. J. Monaghan, *Mon. Not. R. Astron. Soc.* **181**, 375 (1977).
3. R. A. Gingold and J. J. Monaghan, *J. Comput. Phys.* **46**, 429 (1982).
4. J. J. Monaghan and R. A. Gingold, *J. Comput. Phys.* **52**, 374 (1983).
5. J. J. Monaghan, *SIAM J. Sci. Stat. Comput.* **3**, 422 (1982).
6. J. J. Monaghan, *Comput. Phys. Rev.* **3**, 71 (1985).
7. W. Benz, *Numerical Modeling of Nonlinear Stellar Pulsation: Problems and Prospects* (Kluwer Academic, Boston, MA, 1990), p. 269.
8. J. J. Monaghan, *J. Comput. Phys.* **52**, 374 (1983).
9. J. J. Monaghan, *Computer Physics Reports* (North Holland, Amsterdam, 1985), p. 71.
10. J. von Neumann and R. D. Richtmyer, *J. Appl. Phys.* **21**, 232 (1950).
11. J. C. Lattanzio, J. J. Monaghan, H. Pongracic, and M. P. Schwarz, *Mon. Not. R. Astron. Soc.* **215**, 125 (1985).
12. J. C. Lattanzio, J. J. Monaghan, H. Pongracic, and M. P. Schwarz, *SIAM J. Sci. Stat. Comput.* **7** (2), 591 (1986).
13. W. F. Noh, *J. Comput. Phys.* **78** (1978).
14. J. J. Monaghan, preprint, Dept. of Math., Monash University, Clayton, Victoria 3168, 1990 (unpublished).
15. C. Truesdell and W. Noll, in *Handbuch der Physik*, Vol. III, Part 3, edited by S. Flugge (Springer-Verlag, Berlin, 1965), p. 42.
16. W. Herrmann, in *Proceedings, 3rd Int. Conf. on Constitutive Laws for Engineering Materials, Tuscon, AZ, 1991.*
17. L. D. Libersky and A. G. Petschek, in *Proceedings, The Next Free Lagrange Conf., Jackson Hole, WY, 1990*, edited by H. E. Trease, J. W. Fritts, and W. P. Crowley (Springer-Verlag, New York, 1991).
18. G. R. Johnson and W. H. Cook, in *Proceedings, Seventh International Symp. on Ballistics, The Hague, The Netherlands, April 1983.*
19. G. V. Bicknell, *SIAM J. Sci. Stat. Comput.* **12**, 1198 (1991).
20. R. W. Hockney and J. W. Eastwood, *Computer Simulation Using Particles* (McGraw–Hill, New York, 1981).
21. G. R. Johnson and T. J. Holmquist, *J. Appl. Phys.* **64**, 3901 (1988).
22. A. J. Piekutowski, *Int. J. Impact Eng.* **10**, 453 (1990).